ADVANCED FUNCTIONAL MATERIALS
www.afm-journal.de

Polarizable H-Bond Concept in Aromatic Poly(thiourea)s: Unprecedented High Refractive Index, Transmittance, and Degradability at Force to Enhance Lighting Efficiency

Seigo Watanabe, Luca M. Cavinato, Vladimir Calvi, Richard van Rijn, Rubén D. Costa, and Kenichi Oyaizu**

Developing transparent and highly refractive environmentally friendly polymers has not been realized yet toward sustainable optoelectronics. This work describes poly(thiourea)s (PTUs) design following a new "polarizable group synergy" concept, combining highly polarizable hydrogen bonding groups and aromatic-based spacers to form densely packed and high-refractive-index polymer networks. Specifically, PTUs containing *m*- and *p*-phenylene spacers exhibit an easy synthesis, high thermostability (T_g = 159 °C), visible transparency (>92%*T* at 1 µm-film), ultra-high refractive index (n_D = 1.81) based on the random H-bonding arrays with a high packing constant (K_p = 0.738), and straightforward preparation of flexible films via solvent-based techniques. Capitalizing on these assets, PTU-films are integrated into benchmark graphene-based lighting device architectures based on the light-emitting electrochemical cells (LECs) concept. A joint optical modeling and experimental validation confirm the increase in external quantum efficiency expected by the enhanced light out-coupling of PTU-films. Finally, PTUs are efficiently depolymerized to low molecular weight compounds by simply adding diamines under heating, following the dynamic covalent bond exchange between thiourea moieties. Overall, this work highlights the PTU family as new promising materials with a unique polarizable H-bond design to meet efficient and sustainable thin-film lighting devices.

1. Introduction

High refractive index polymers (HRIPs), which generally denote polymers with refractive index (RI) over 1.7, are attractive materials to improve the performance or efficiency of various optical components.[1–4] Especially, optoelectronic devices, including organic light-emitting diodes (OLEDs) and light-emitting electrochemical cells (LECs), are major applications that require ultra-high refractive index thin-film layers with adequate transparency in order to realize efficient light-to-energy conversion by enhancing photon-extraction efficiencies.[5–7]

A basic strategy to design highly refractive polymers is to introduce substituents with high molar refraction ([*R*]) and/or minimize the total volume of the materials in the bulk state based on the Lorenz–Lorenz equation.[1,8,9] To date, general HRIPs have been designed with the former strategy by incorporating mainly sulfur groups.[10–12] Though some HRIPs, including inverse-vulcanized polymers[13,14] and heavy-chalcogenide polymers,[15,16] have shown outstanding RI over 1.8, they are not visible-transparent and hindered their practical applications. Such transparency-RI dichotomy is explained by the Kramers–Kronig relation, in which excessively high-[*R*] groups contribute to the red-shifting of absorption bands with large π-electron distribution (i.e., small HOMO-LUMO gaps), resulting in film coloration.[9,17] This can be circumvented with a sulfur chemical vapor deposition (sCVD) method, which yields thin films with RI over 1.9 and low

S. Watanabe, K. Oyaizu
Department of Applied Chemistry and Research Institute for Science and Engineering
Waseda University
Tokyo 169-8555, Japan
E-mail: oyaizu@waseda.jp

The ORCID identification number(s) for the author(s) of this article can be found under https://doi.org/10.1002/adfm.202404433

DOI: 10.1002/adfm.202404433

L. M. Cavinato, R. D. Costa
Chair of Biogenic Functional Materials
Technical University of Munich, TUM Campus Straubing for Biotechnology and Sustainability
Schulgasse 22, 94315 Straubing, Germany
E-mail: ruben.costa@tum.de

V. Calvi, R. van Rijn
Applied Nanolayers B.V.
Feldmannweg 17, 2628 CD Delft, The Netherlands

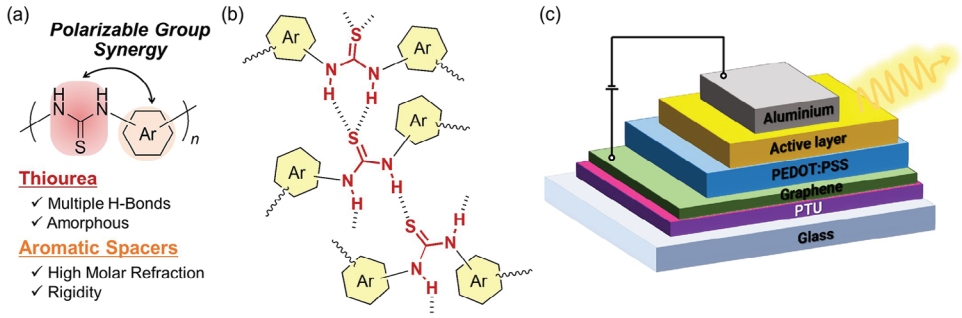

Figure 1. Research concept. a) Molecular design of **PTU**s with "polarizable group synergy". b) Plausible schematic representation of disordered (various conformational) H-bonding networks between the **PTU** chains enabling polarizable supramolecular networks (Note: This diagram has assumption that thiourea can form H-bonds with various binding angles, based on the previous literature).[25] c) Schematic representation of the architecture of LECs devices.

coloration. However, this approach is not cost-effective and versatile, resulting in films that are difficult to process in solution. In contrast, we have recently focused on the free volume reduction strategy to realize polymers with even higher RI and visible transparency via non-covalent interactions. The representative example is poly(phenylene sulfide) (PPS) with monohydroxy group, exhibiting unprecedented optical properties with ultra-high RI (above 1.80) and an amorphous structure ascribed to the intermolecular H-bonds partially restricted by rigid PPS chains.[18] By extending this concept to sulfur-rich[19] or dihydroxy-substituted[20] PPS derivatives, RI finally reached up to n_D = 1.85 based on their increased refractivity per unit volume. As various non-covalent interactions widely range in the aspect of bonding strength and reversibility, there would remain huge space for unexplored ultra-high RI polymers to which our strategy is applicable. Among them, multiple H-bond is a promising choice for enhancing supramolecular-crosslinking density as typically used for reversible responsive materials.[21,22] However, excessive multiple H-bonds generally lead to crystalline or inhomogeneous (phase-segregated) structures,[23,24] compromising the final transmittance of their optical materials.

In light of the above prior art, the design of polymers meeting high refractive and transparency, moderately high polarizability, strong intermolecular interactions for minimizing free volume, random polymer chain conformation, and eco-designs (i.e., biogenic, biodegradable, and/or recyclable) still remains as a major challenge in the field. Herein, we met these concepts in thiourea-based polymer derivatives, exploiting an exceptional multiple H-bonding motif that enables disordered arrays based on its large electron distribution around the sulfur atoms.[25] These features resulted in its densely packed network structures with amorphous properties,[26,27] leading to their attractive bulk properties for self-healable polymer glasses,[27,28] Li^+ superconductors,[29] metal absorption polymers,[30] covalent adaptable networks,[31] and dielectric materials.[32–34] Though RI of a few thiourea-containing polymers were measured as a guideline for evaluating their dielectric constants,[35] detailed investigations for transparent optical materials including HRIPs have not been reported yet.

This work demonstrates aromatic poly(thiourea)s (**PTUs**) as an efficient candidate for ultra-high RI polymers realized by "polarizable group synergy" concept design. Here, the polarizable thiourea contributed to build up dense yet amorphous multiple H-bonding networks with reduced free volume, in concert with high RI enhanced through the combination with high-[*R*] aromatic spacers (**Figure 1**). This resulted in outstanding optical features, such as visible transparency (> 92%*T* at 1 μm-film) and ultra-high refractive index (n_D = 1.81) along with an easy flexible film forming via solvent-based techniques, by adopting the most compact phenylene spacers that allowed easy H-bonding between thioureas to increase the packing density. A joint theoretical modeling and experimental validation further confirmed their technological relevance to enhance the light out-coupling in thin-film LECs, maximizing the external quantum efficiency (EQE) in benchmark device architectures embedding graphene electrodes. Finally, these **PTUs** also exhibit an easy degradability when exposed to diamines, leveraging the bond exchange properties inherent in thioureas.

All-in-all, this work discloses a new family of **PTU**s with unprecedented optical features to enhance light out-coupling, while they are also well-aligned with green principles. This combination is a significant stride toward sustainable photon-manipulation for optoelectronic and photonic purposes, in general, and thin-film lighting devices, in particular.

2. Results and Discussion

2.1. Synthesis and Properties of Aromatic Poly(thiourea)s

2.1.1. Synthesis and Crystalline Properties

The target poly(thiourea)s were synthesized by either polyaddition of the corresponding diamines and diisothiocyanates or polycondensation of the diamines with 1,1′-thiocarbonyldiimidazole as C=S source, by referring to the previous reports.[27,33] For pursuing polymers with excellent optical properties, we designed six aromatic-based **PTU**s and categorized with three groups: **Phenylene-PTU**s with maximized thiourea content (***m*Ph-PTU**, ***mp*Ph-PTU**), **Sulfide-PTU**s with high-[*R*] (**PhSPh-PTU**, ***p*PhPPS-PTU**), **Rigid-PTU**s with a biphenyl (**diMeBiPh-PTU**) and a cardo-based fluorene skeleton (**Flu-PTU**) (**Figure 2**). The resulting polymers were high molecular weight (M_w over 10^4)

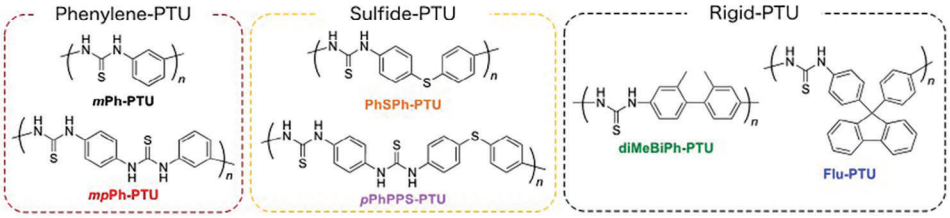

Figure 2. Structure of poly(thiourea)s synthesized in this study.

and soluble only in polar amide solvents such as N,N-dimethylformamide (DMF), Dimethyl sulfoxide (DMSO), and N-methyl-2-pyrrolidone (NMP), ascribed to the H-bond rich structures. Their structures were characterized by ^{1}H, ^{13}C NMR, and IR spectroscopy (Figures S1–S18, Supporting Information). All the ^{1}H NMR spectra showed signals consistent with the corresponding repeating structures, especially at ≈10 ppm observed the N—H signals for thiourea units. The IR spectra revealed two vibration modes for H-bonding N—H groups (linear H-bonding N—H stretching and nonlinear H-bonding N—H deformation vibrations).[27]

Next, we examined crystalline and thermal properties. From the XRD profiles, no diffraction peaks were observed for all **PTU** even in the presence of hydrogen bonding networks owing to their random conformations (Figure S19, Supporting Information). We further examined the microstructures by thermogravimetric analysis (TGA) and differential scanning calorimetry (DSC), whose thermograms showed a slight exothermic peak ranging in 76–89 °C (except for ***p*PhPPS-PTU**) and a baseline shift ranging in 148–203 °C (except for **PhSPh-PTU**) for each **PTU** (Figures S20 and S21, Supporting Information). These thermal transitions have been ascribed as a micro-Brownian motion of flexible thiourea arrays (i.e., melting/reconstruction of the H-bonds of thiourea arrays) and glass transition of rigid aromatic backbones, respectively. Also presumably, the exceptional thermal transition of **Sulfide-PTU**s was ascribed to the strong π–π stacking of PhSPh unit, which increased T_g toward over thermal degradation temperature for **PhSPh-PTU** while alternatingly phenylene-containing ***p*PhPPS-PTU** weakened the π–π stacking whereas prevented the micro-Brownian motion due to less unit regularity. Therefore, **PTU**s in this study were amorphous in a broader sense, where small nano-sized crystals that were undetectable from the XRD profiles remained as thiourea segments in the solid state. On the other hand, ***mp*Ph-PU**, a polyurea analog of ***mp*Ph-PTU**, showed strong diffraction peaks in the XRD profile, which were correlated with the trans/trans-type (linear) dominant H-bonds from the IR spectrum (Figure S22, Supporting Information). Therefore, thiourea moieties can disorganize the linear H-bonding-derived crystalline region thanks to the cis/trans-type (nonlinear) H-bonding, contributable to preventing macroscopic agglomeration of the polymer chains.

2.1.2. Optical Properties

Optical properties for **PTU**s were also investigated in thin films and the solution states. Transparent thin films of **PTU** were prepared via wet-processing of their DMF or DMF/DMSO solutions (**Figure 3**a). Especially the ***mp*Ph-PTU** film can be peeled off from the substrate and was not fractured upon bending (Figure 3b). This strongly contrasts with the brittle features of previous aromatic-based ultra-high-RI polymers (e.g., PPS derivatives).[18–20] Such flexibility is attributed to the dense and disordered H-bonds of thiourea units that were especially strengthened in the case of the ***mp*Ph-PTU** with the most robust and dense H-bonding (see section 2.3 for details). The UV–vis spectroscopy represented no absorption of the **PTU** solutions in the visible-light region (Figure 3c). While highly polarizable **Sulfide-PTU**s showed the longest cut-off wavelength, the **PTU** containing the *p*-phenylene spacer (***mp*Ph-PTU**) represented blue-shifting of the absorption with higher transparency whereas ***m*Ph-PTU** or **Rigid-PTU**s were even more transparent based on their less polarizable spacers. Also, this trend in solution was consistent with the film transparency (Figures S23 and S24, Supporting Information), representing no reduction in transparency without any scattering at large wavelength (ca. 500–800 nm). Furthermore, **PTU**s showed higher transparency over 88%*T* (with 1 µm thickness, normalized) in the visible-near infrared (NIR) region, and the transparency was greatly improved for **Phenylene-** (above 92%*T*) and **Rigid-PTU**s (above 95%*T*) corresponding to the unit polarizability.

RI of **PTU**s resulted in n_D (RI at 589 nm) = 1.72–1.83 with Abbe numbers of ν_D = 11–18 (Figure 3d), representing similar or superior RI properties to the representative sulfur-containing HRIPs (e.g., alkyl/alkoxy-substituted PPS (n_D = 1.69–1.75)[9,20,36] and triazine-containing PPS (n_{633} = 1.7112-1.7530)).[37,38] The detailed RI for each **PTU** also depends on the spacer structure, which was in the contrary relationship to the trend for UV–vis absorption. In particular, **Phenylene-PTU**s and **Sulfide-PTU**s resulted in higher RI (≈1.8) based on their high thiourea and sulfur content, in contrast to **Rigid-PTU**s with n_D below 1.75. Also, ***mp*Ph-PTU** especially possessed higher molecular weight and higher T_g among ultra-high RI **PTU**s in this study, while representing similar film absorptivity compared to the previous ultra-high RI polymers (Table S3, Supporting Information). The superior properties of ***mp*Ph-PTU**, including its flexibility as shown in Figure 3b, make it a favorable choice for applications involving visible-transparent optical thin films, such as encapsulants for flexible thin-film lighting devices to enhance light-outcoupling based on their RI closer to the values for conventional transparent electrodes (e.g., graphene: $RI_{(590\ nm)}$ = 2.69 and ITO: $RI_{(590\ nm)}$ = 1.90),[39] compared with traditional transparent HRIPs with RI ≈ 1.7.

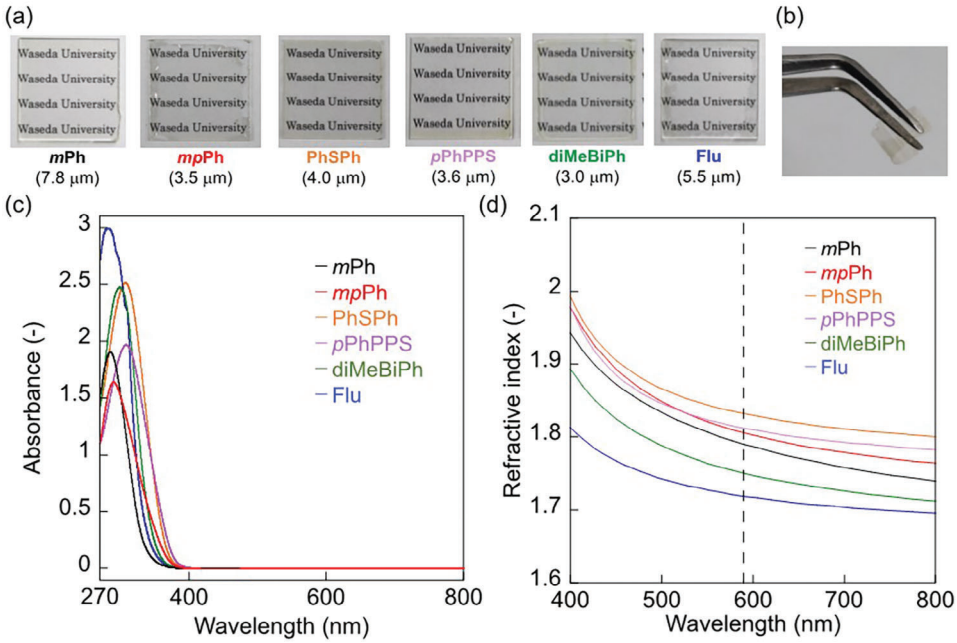

Figure 3. Optical properties of **PTU**s: a) Photographs and thickness (Parentheses) for the PTU thin films on glass substrates. b) Flexible free-standing ***mp*Ph-PTU** thin film upon bending with a tweezer. c) UV–vis absorbance spectra of 0.1 mM **PTU** solutions in DMF. The UV–vis spectra of the **PTU** films were represented in Figures S23 and S24 (Supporting Information). d) Refractive indices of **PTU**s.

2.2. Validation Concept: Elucidating Intermolecular Interactions of Poly(thiourea)s

For further understanding structure-property relationships regarding PTUs, we investigated the structural information in the solution/films focusing on the H-bonds of thiourea units. To clarify the H-bonding behavior, we conducted ^{1}H variable temperature (VT)-NMR measurements, in which only the N—H signals of thiourea showed up-field shift for all PTUs with increasing temperature. The shifting rate was determined as $\approx -4 \times 10^{-3}$ ppm K^{-1} regardless of the spacer structure, which were in the range of intermolecular H-bonds (**Figure** 4a,b; Figure S26 and Table S4, Supporting Information).[40] Only for ***mp*Ph-PTU** were confirmed two N—H signals of thiourea, which were observed when the conformational change between trans/trans and cis/trans is slower than the timescale of ^{1}H NMR,[41] representing its more robust H-bonding features (i.e., requiring longer conformational changing time) in contrast to the other **PTU**s. This behavior was consistent with the highest packing constant of ***mp*Ph-PTU** (vide infra). Such intermolecular H-bonds were present even in the solid states, confirmed from the solid-state NMR with the clear down-field shift of the thiocarbonyl signal (ca. at 180 ppm) (^{13}C, Figure 4c) and the up-field shift of the N—H signal (^{1}H, Figure S27, Supporting Information) upon heating (Note: the solid-state ^{1}H spectrum represented well-broadened signals due to strong dipolar-dipolar interactions). Subsequently, we examined the H-bonds in the solid states from the IR spectra. In films, the signals for the trans/trans type H-bonding N—H stretching were drastically red-shifted than in the case for powder states, whereas the signal for free N—H bonds was simultaneously decreased (Figure 4d,e). In addition, the cis/trans type H-bonding N—H deformation vibration, which were characteristic bands of not urea but thiourea groups,[27] were detected with red-shifting in the film state for **Phenylene-PTU**s, whereas no significant shifts were found for the other **PTU**s. Such spectral change describes the uniform and more widespread H-bonding network of **PTU**s upon the film formation, whose effect is especially remarkable for the case with the compact spacers. The conformational ratio of trans/trans H-bonds ranged from 0.60 to 0.72 in the powder states, whereas the value was mostly the same (≈0.6–0.8) even in the film states (Figure S28, Supporting Information). The H-bonding array of thiourea slightly favors a linear conformation rather than the zigzag cis/trans structure, but the cis/trans type H-bonds disrupted the ordered H-bond networks to avoid micro phase-separated domains despite the preferential trans/trans type H-bonds, resulting in high transparency of **PTU**s.

We further investigated the packing features for **PTU**s in the solid states via density measurements, in which the packing constants (K_p) were evaluated (**Figure** 5a). Except for **PhSPh-PTU** and **Flu-PTU**, the **PTU** chains were densely packed with K_p over 0.681, which was the empirical value for general amorphous polymers.[42] The multiple H-bond networks between thiourea units enhanced chain packing regardless of the spacer structures. Among the **PTU**s reaching or coming close to the ultra-high RI (ca. 1.8), **Phenylene-PTU**s (red bracket in Figure 5a) represented the highest K_p than **Sulfide-PTU**s (orange bracket), which showed that the dominant factor of achieving ultra-high RI was high sulfur content for the **Sulfide-PTU**s and high K_p for the **Phenylene-PTU**s, respectively. Moreover, such intense chain-packing of **Phenylene-PTU** was attributed to the compact structure of phenylene spacers, which allowed closer contact between thiourea arrays regardless of their conformations; for instance, this peculiar feature also can explain their exceptional

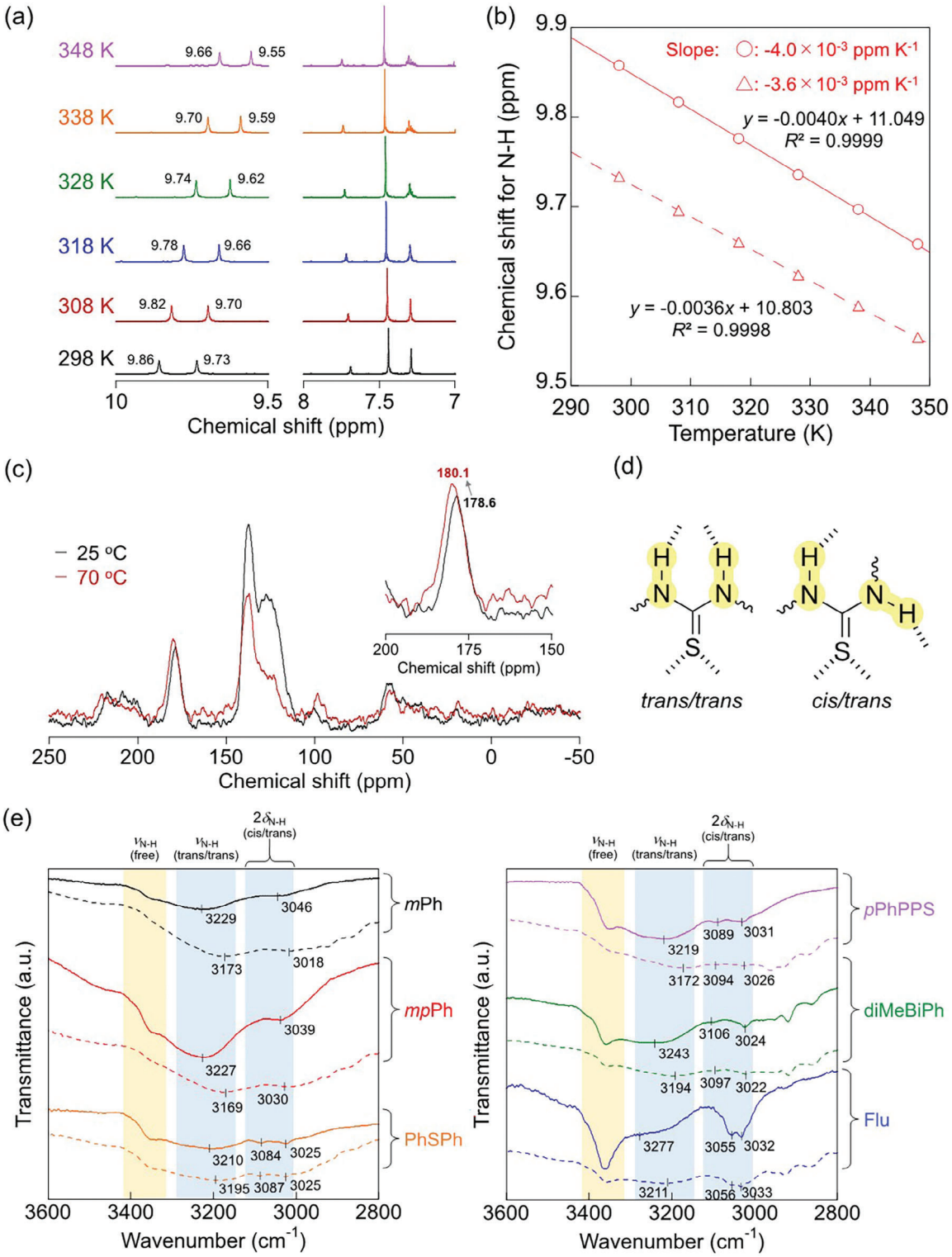

Figure 4. Investigating H-bonds of **PTU**s in the solution and the bulk states. a) Expanded ^{1}H VT-NMR spectra for ***mp*Ph-PTU** in DMSO-d_6 at 298, 308, 318, 328, 338, and 348 K. Two signals for N—H groups were observed due to the conformational change of cis/trans and trans/trans conformations during the NMR measurements.[41] b) Correlation between temperature and chemical shift for N—H (thiourea) signals in the solution VT-NMR spectra for ***mp*Ph-PTU**. Only the signals for N—H bonds were shifted in accordance with the temperature change. c) Solid-state CP/MAS ^{13}C VT-NMR spectra for ***mp*Ph-PTU** at 25 and 70 °C. Upon heating, the signal for thiocarbonyl groups (at ca. 180 ppm) was shifted to the downfield. d) two conformation states of the multiple H-bonds for thiourea. e) IR spectra of the **PTU**s in the powder (solid lines) and the bulk (dotted lines) states. Yellow and blue brackets corresponded to the absorption bands for free and H-bonded N—H vibration modes, respectively.

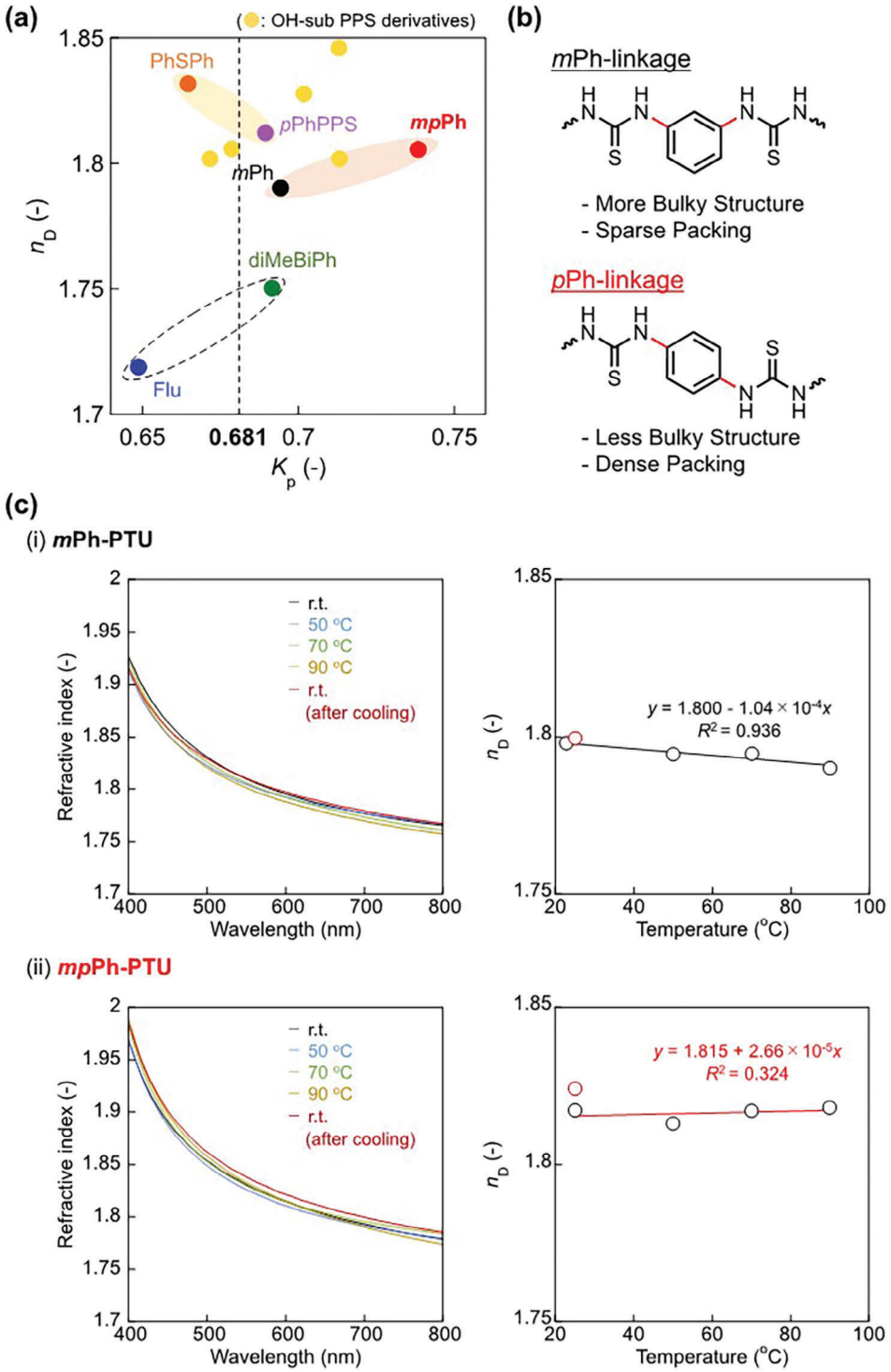

Figure 5. Packing features of **PTU**s. a) Correlation between n_D versus K_p for **PTU**s and ultra-high RI polymers with single H-bonds (hydroxy-containing PPS derivatives).[19] Orange, yellow, and black brackets categorize **Sulfide-PTU**, **Phenylene-PTU**, and **Rigid-PTU**, respectively. b) Schematic representation of *m*-Ph and *p*-Ph linkages including their packing features. c) VT-spectroscopic ellipsometry for **Phenylene-PTU**s: (left) RI spectra. (right) n_D-temperature relationship. Red plots represented n_D values after cooling from 90 to 25 °C.

red-shifting of $2\delta_{cis/trans}$ band upon film formation in Figure 4e (vide supra). On comparing **Phenylene-PTU**s, ***mp*Ph-PTU** with the alternating *m*- and *p*-phenylene linkage led to much higher K_p (0.738) than ***m*Ph-PTU** as well as the other **PTU**s. As *p*-phenylene spacer connected straightly to the adjacent thioureas, more densely H-bonded thiourea arrays were constructed in the bulk states compared with the case for only the *m*-phenylene group with a bent linkage. Based on the above structure-property relationships for **PTU**s, we conclude that the **Sulfide-PTU** skeleton resulted in high RI but poor visible transparency for its excessively high polarizability, while the compact **Phenylene-PTU** skeleton with linearly connected adjacent thioureas resulted in high RI as well as the maintained high transparency based on its enhanced H-bonding density. Additionally, ***mp*Ph-PTU** exhibited higher K_p than the previous OH-containing PPS derivatives[19] with single H-bonding moiety (yellow plots in Figure 5a), representing the synergistic effect of compact spacers and multiple H-bonded thioureas for achieving denser H-bond networks.

To verify the heating/humidity tolerance of H-bonds including their effect on RI, temperature/humidity dependence was investigated. First, VT-ellipsometry techniques were conducted to measure the RI-temperature relationships for all **PTU**s (Figure 5c; Figure S30, Supporting Information). The coefficient for temperature-n_D plots was generally negative upon heating, while only ***mp*Ph-PTU** exceptionally represented a positive value. This anomalous trend was based on the highest K_p and the spacer compactness of ***mp*Ph-PTU**, which allowed the rapid annealing of dense and robust thioureas under mild heating conditions around T_{en}, resulting in smaller free volume. After cooling the heated sample to room temperature, the n_D for **Phenylene-** and **Sulfide-PTU**s were surprisingly enhanced compared with the original n_D prior to heating, whereas those for **Rigid-PTU**s resulted in lower values. Upon cooling, the polymer chains were frozen after annealing by the micro-Brownian motion to decrease free volume, while **Rigid-PTU**s did not benefit from the effect due to their large free volume derived from the bulky spacers. Next, we measured the humidity-dependence of the RI for ***mp*Ph-PTU** by comparing the ellipsometry results before and after the humidity exposure. Despite the dense H-bond-containing structures, ***mp*Ph-PTU** can maintain RI of ca. 1.8 even after a long-term (24 h) exposure with a slight decrease (< 0.01) (Figure S31, Supporting Information), suggesting enough humidity tolerance at a practical level. Toward higher humidity tolerance, introducing another orthogonal hydrophobic interaction[28] in the **PTU** spacer skeleton would be contributable.

2.3. Validation Concept: Demonstrating Light-Amplifying Layer for Lighting Devices

The bottom-emitting device architecture was selected—see experimental section for further details and Figure 1c, while the discussed data is based on up to 20 devices. In short, the anode consisted of a ***mp*Ph-PTU** films prepared onto glass substrate (1.5 mm, incoherent) via spin-coating followed by solvent-transfer deposition of a graphene electrode (1 nm, coherent). The active layer was prepared via spray-coating of first PEDOT:PSS (coherent) followed by spin-coating of the benchmark $[Ir(dtbbpy)(ppy)_2]PF_6$ and SuperYellow (SY) emitters (90 nm, coherent).[43] The cathode was prepared via physical vapor deposition of aluminum (100 nm, coherent). The refractive indices of the complete device stack on one side of the transparent electrode and the ***mp*Ph-PTU** layer on the other side are similar so that the only significant optical interface remaining is between ***mp*Ph-PTU** layer and the glass substrate.[44] The outcoupling enhancement of the device structure was simulated based on the dipole emission model and the transfer matrix method using Setfos 5.3 simulation software.[45,46] Prior to device fabrication, topography images of spin-coated ***mp*Ph-PTU** were acquired to ensure the morphological requirements. In all the cases, root mean square roughness <1 nm has been found—Figure S32 (Supporting Information). **Figure 6a** shows the simulated outcoupling efficiency (η_{OC}) for an Ir-based LECs with respect to different thicknesses of PEDOT:PSS and ***mp*Ph-PTU** layers, keeping constant the thicknesses of the other layers—vide supra. Peak enhancement is met for ***mp*Ph-PTU** films of 25 nm with a PEDOT:PSS layer between 120–130 nm. This corresponds to a potential increase of 5% of the EQE. Experimental confirmation was carried out by analyzing luminance–current–voltage (LIV) assays of devices without ***mp*Ph-PTU** (reference) and devices with ***mp*Ph-PTU´s** layer thickness of 28 and 75 nm—Figure 6b. In perfect agreement with the simulations (Figure 6c), the average maximum luminance increased from 252 cd m^{-2} (reference) to 310 cd m^{-2} (***mp*Ph-PTU**; 28 nm), corresponding to an increase of 5% in the total EQE. In addition, all devices showed a yellow electroluminescence response consisting of a broad and structureless emission band centered at 560 nm (Figure 6d), confirming the lack of any color corruption by the introduction of a highly transparent ***mp*Ph-PTU** layer. Next, device stability was studied using a pulsed current scheme at 50 mA cm^{-2}, block-wave at 1 kHz, and a duty cycle of 50% to demonstrate their correct operational mode—Figure S33 (Supporting Information). In short, the devices showed the typical LEC behavior: an initial voltage (ca. 5.0 V) that exponentially reduces to a plateau at lower values, while the luminance rises from an initial value of ca. 50 cd m^{-2} to a maximum of ca. 250/350/300 cd m^{-2} for devices fabricated with a ***mp*Ph-PTU** layer of 0 (a), 28 (b), and 75 (c) nm, respectively. Noteworthy, the quick (<10 min) decrease of the average voltage is related to a healthy electrochemical doping promoted by the formation of electric double layers at the electrode interfaces. After ca. 20 h, a drop in the luminance level was recorded, ending up in a $t_{1/2}$ (time to reach half of the maximum luminance) of >120 h for all the cases, confirming state-of-art LECs performances with respect to graphene based devices.[43,47,48]

Finally, to validate further the proposed light enhancement a second archetypal emitter has been tested, namely SY. Active layer of SY and tetrahexylammonium tetrafluoroborate ($THABF_4$) 10% wt. have been spin coated on top of the PEDOT:PSS layer (100–110 nm). In this configuration, a theoretical maximum EQE enhancement of 12% is possible employing 45 nm thick layer of ***mp*Ph-PTU**—Figure S34 (Supporting Information). Experimental validation through luminance–current–voltage (LIV) assays supports these findings, revealing a 12.4% total EQE increase with 52 nm ***mp*Ph-PTU**.

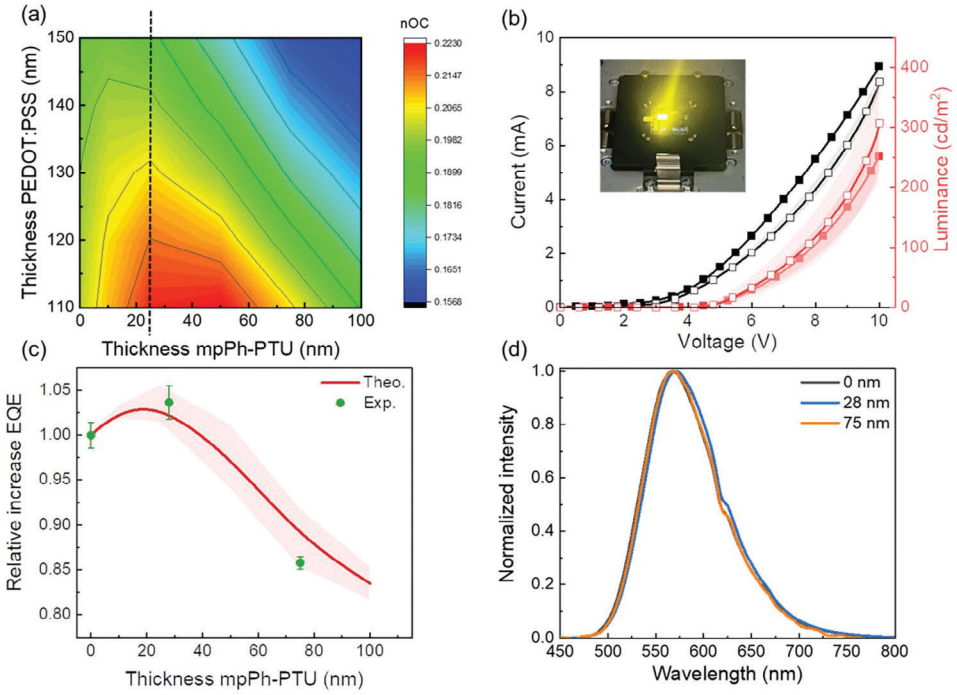

Figure 6. a) Simulated values of light-outcoupling efficiency for several thicknesses of PEDOT:PSS and ***mp*Ph-PTU** layers. The dashed line corresponds to 25 nm thickness. b) LIV characteristics of LECs fabricated without ***mp*Ph-PTU** (full symbols) and with ***mp*Ph-PTU** film of 28 nm (open symbols). The inset shows a picture of a device in operando. c) Comparison of calculated and experimental values of EQE versus ***mp*Ph-PTU** thickness showing outcoupling enhancement at ca. 25 nm. Enhancement ratios are based on theoretical results obtained from the Setfos simulation software. d) Electroluminescence spectra recorded at peak luminance.

2.4. Validation Concept: Establishing an Easy-to-Degrade Protocol

Due to recent environmental issues caused by plastic wastes, degradation of polymers to monomers becomes one of the essential functionalities leading to sustainable recycling. To the best of our knowledge, the only attempt to impart degradability to HRIPs is the recyclable poly(trithiocarbonate)s by Ren et al.[49] In addition, systematic design for degradable HRIPs has not been proposed before in spite of such global request.

To afford degradability targets, a molecular design that enables chain cleavage under the presence of external trigger is necessary.[50–53] As thiourea is a dynamic covalent bond that reversibly dissociates to the corresponding amines and isothiocyanates, especially under the base-catalyzed heating conditions,[31,54–56] we anticipated that **PTU** can be degraded to low-molecular-weight compounds using the excessive diamines (**Figure 7a**). The degradation behavior of thiourea-containing thermoset has been reported,[55] but due to their insolubility ascribed to the cross-linking structure, only the molecular weight of the degraded products was provided and the detailed degradation mechanism has still been unveiled. Here, we revealed for the first time that the excessive diamine behaves as both the catalyst and the end-capping agent of isothiocyanate groups for cleaving the **PTU** chains.

We selected ***mp*Ph-** and ***p*PhPPS-PTU** for the degradation tests because these polymers showed the most efficient potentials with ultra-high RI as well as high molecular weight and high solubility in DMF. Each **PTU** was stirred with or without excess *m*-phenylenediamine (*m*PDA) in DMF at room temperature or under heating (at 50 °C) and molecular weights were monitored by SEC (Figure 7c,d, Figure S35b,c, Supporting Information). On the degradation of ***mp*Ph-PTU** (M_n = 2.7 × 10^4), both the addition of *m*PDA and heating accelerated the degradation reaction owing to the rapid bond exchange reactions. For entry 1 in Figure 7b (diamine addition + heating), ***mp*Ph-PTU** was instantly depolymerized and finally reached the lowest M_n of 1.8 × 10^3 (Figure 7e) with the highest degradation efficiency (i.e., conversion of thiourea) of 91% after 72 h (**Figure 8**). According to the ^{1}H NMR spectra of the degraded fraction, new signals for thiourea, phenyl, and amino groups were confirmed in conjunction with the degradation (Figure 7g; Figures S36–S38, Supporting Information). After the molecular weight was saturated, most of these signals can be characterized as the protons of the terminal structures that can be observed only after the end-capping by *m*PDA, whereas there were several unidentifiable signals (e.g., the signal at 6.72 ppm, between proton **e** and the *m*PDA signals) assignable as incompletely degraded products. These SEC and NMR results supported the main-chain degradation mechanism, in which the additive diamines were selectively inserted into the isothiocyanate terminal of the degraded **PTU** fragment during the bond exchange reaction (**Figure 9a**, black and red brackets). This selectivity was observed because the terminal amine of **PTU** exhibited lower nucleophilicity than the aromatic diamine. This difference can be attributed to the electron-withdrawing effect of the adjacent thiourea moiety on the aminophenyl unit within the **PTU** chain.

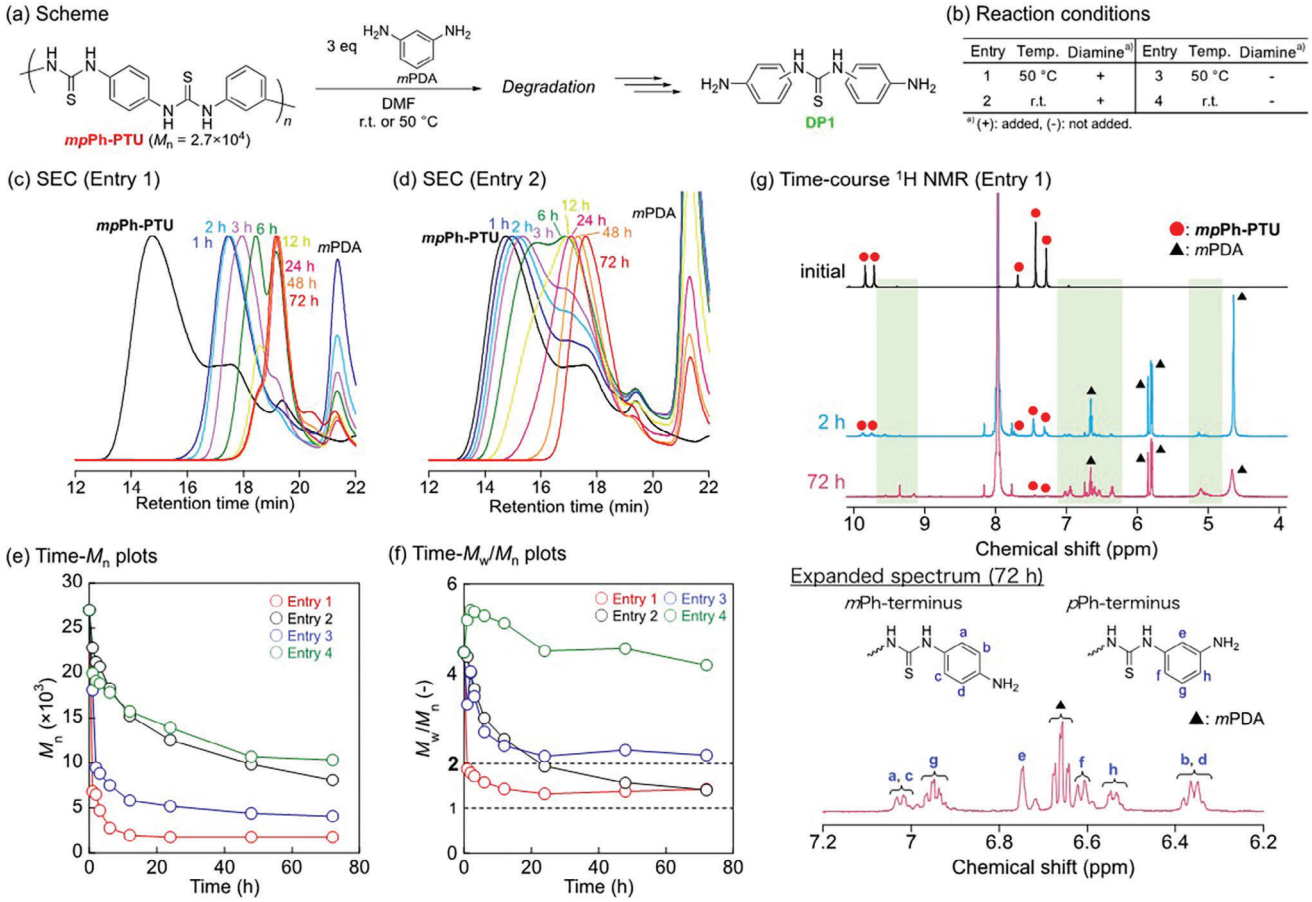

Figure 7. Time-course for the degradation of ***mp*Ph-PTU**: a) Degradation scheme of ***mp*Ph-PTU**. b) Reaction conditions. c) SEC chromatograms of the fractionated products for entry 1 (at 50 °C, with diamine) in DMF (with 10 mM LiCl). d) SEC chromatograms for entry 2 (at room temperature, with diamine). e) Time-M_n plots. f) Time-M_w/M_n plots. g) ^{1}H NMR spectra (initial, 2 and 72 h) including the expanded spectrum (72 h) for entry 1. Other time-course spectra were displayed in Figure S36 (Supporting Information).

Upon stirring ***mp*Ph-PTU** without diamine (entries 3 and 4 for Figure 7b), the molecular weight of **PTU** also decreased although the degradation was suppressed compared with the corresponding entries 1 and 2. Especially for the heating condition (entry 3), the molecular weight reduced significantly and was finally saturated with a higher value than entry 1 ($M_n = 4.1 \times 10^3$) (Figure 7e, blue line). The molecular weight distribution (M_w/M_n) also decreased in concordance with the degradation progress, and especially for entry 3, M_w/M_n was saturated at ≈2 (Figure 7f, blue line), corresponding to the ideal distribution for step-growth polymerization.[57] Such time-course was similar to the case of dynamic covalent polymers,[58] in which the polymer chains were reconfigured to the most randomized distribution via the repetition of bond exchange reactions. As there were no other signals except for the repeating and terminal structures in the time-course ^{1}H NMR spectra (Figures S39 and S40, Supporting Information), only bond exchange reaction occurred under heating without diamines. This bond exchange reaction for ***mp*Ph-PTU** took place even in the bulk conditions upon heating, confirmed by the decline of molecular weight under no weight loss (Figures S41 and S42, Supporting Information), whereas the degradation rate was much slower than in the solution. The degradation/redistribution of ***p*PhPPS-PTU** also resulted in the same trend (Figures S43–S49, Supporting Information). Summarizing the above degradation/redistribution features, heating **PTU** solutions without additives reached the bond exchange to the equilibrium yielding middle-MW products with $M_w/M_n \approx 2$ (Figure 9bi), whereas heating with diamines gave low-MW products with low molecular weight dispersion ($M_w/M_n \approx 1$–1.5) (Figure 9bii).

In summary, we have precisely demonstrated the switchable degradation system of **PTU**s via dynamic covalent chemistry for the first time. In this system, the required condition was just heating with diamines, which was milder than the previously reported systems. On the other hand, the degradation rate and the E_{deg} values should be improved toward the rapid monomer recovery cycles for practical closed-loop recycling of **PTU**s (**Figure 10**; Table S6, Supporting Information). For instance, adjusting the equilibrium state for dynamic covalent chemistry would increase the E_{deg} values, yielding a higher **DP1** recovery ratio, and utilizing more nucleophilic degradation triggers (i.e., aliphatic diamines) or additional base catalysts also contribute to even rapid degradation rate. Furthermore, the preciseness of the degradation should also be improved so as not to occur the redistribution of **PTU**s even in the absence of diamines. For overcoming such issues,

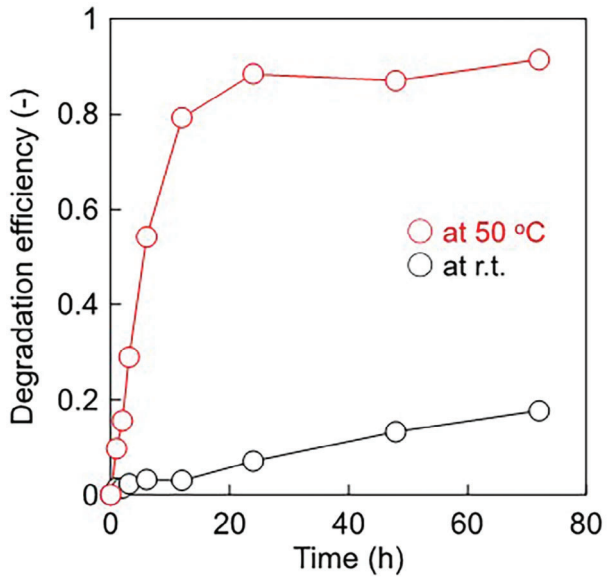

Figure 8. Degradation efficiency of ***mp*Ph-PTU** for entries 1 (at 50 °C) and 2 (at r.t.). Entry numbers corresponded to those in Figure 7b.

enhancing bond-dissociation energy of C—N bonds for thiourea, which is a driving force of bond exchange reaction,[54] should be precisely tuned through the introduction of electron-deficient side groups or heteroaromatic spacers into the present **PTU**s.

3. Conclusion

We have demonstrated transparent, ultra-high refractive, and easy-to-degrade poly(thiourea)s (**PTU**s) films following a new polymer structure concept to overcome the current empirical RI-transparency dichotomy: the first combination of highly polarizable hydrogen bonding groups and aromatic-based spacers to form densely packed, transparent, and high-refractive-index polymer films. In detail, we have synthesized six aromatic poly(thiourea)s (**PTU**s) from conventional diamines under mild conditions with high molecular weight, well solution-processability, and thermal properties. Notably, the compact phenylene-containing **PTU** achieved the highest density and packing constant (1.50 g cm^{-3}, K_p = 0.738), high visible transparency (over 92%T at 1 μm), and an ultra-high RI (n_D = 1.81). These fascinating properties were attributed to the "polarizable group synergy", whereby multiple H-bonding thioureas and phenylene spacers have contributed cooperatively to achieving amorphous, dense, and high-RI polymer networks based on their high polarizability. The **PTU** films were further implemented as a light-amplifying layer in LECs, resulting in the expected improved efficiency upon compensating RI mismatching between the glass-electrode interfaces as corroborated by optical simulations without affecting device stability. Importantly, other device configurations, such as Glass/**PTU**(110 nm)/ITO/PEDOT/Emitter/Al, should also lead to even higher EQE increase of up to 15% as simulated with Setfos 5.3 (Figure S50, Supporting Information). Finally, **PTU**s are dynamic covalent polymers, allowing us to easily degrade them to their low molecular weight components by simply just adding diamine to the solution upon heating. While this study demonstrates only the degradation of **PTU**, the diamino-terminated degraded products can be recycled as diamine monomers to synthesize various **PTU** and other functional polymers (e.g., polyimides) (Figure 10, gray part). Also, considering that polyaddition synthesis of **PTU** produces no byproducts, this depolymerization/re-polymerization system can be regarded as a solution for realizing closed-loop recycling of HRIPs. This concept should be expandable to developing new HRIPs with sulfur-based degradable skeleton.[59] Overall, this is the first step toward the comprehensive design of a next-generation optoelectronic polymers achieving high light-extraction efficiency and environmental friendliness.

4. Experimental Section

Materials: 1,3-phenylenediamine (*m*PDA), 1,4-phenylene diisothiocyanate, bis(4-aminophenyl sulfide), *m*-tolidine, 9,9′-bis(4-aminophenyl) fluorene were purchased from Tokyo Chemical Industry Co. Dimethyl sulfoxide (DMSO), N-methyl-2-pyrrolidone (NMP), N,N-dimethylformamide (DMF) were purchased from Kanto Chemical Co. 1,1′-thiocarbonyl diimidazole was purchased from Sigma–Aldrich Co. Methanol was purchased from Kokusan Chemical Co. All reagents were used as purchased without further purification.

Measurements: ^{1}H (500 MHz) and ^{13}C (125 MHz) NMR spectra were recorded by JEOL JNM-ECX500 or ECZ500. Fourier-transform infrared (IR) spectra were recorded by JASCO FT/IR-6100 with KBr pellets or with the attenuated total reflection (ATR) method (attached kit: JASCO ATR PRO ONE). Variable temperature NMR (VT-NMR) measurements (600 MHz) were conducted by Bruker AVANCE 600 NEO. Size extrusion chromatography (SEC) was conducted with SHIMADZU LC-20AD/CBM-20A using TOSOH TSK-GEL column with SHIMADZU SPD-M20A UV detector (wavelength: 275 nm) (eluent: DMF with 10 mM LiCl, flow rate: 0.3 mL min^{-1}, molecular weights were calibrated by polystyrene standards). Differential scanning calorimetry (DSC) was conducted with TA Instruments Q200. UV–vis spectra were recorded by Jasco V-670 spectrometer. For the UV–vis measurement of polymer solutions, a quartz cell with 1 cm length was used. Spectroscopic ellipsometry was conducted by HORIBA UVISEL ER AGMS iHR320. The density of the polymer samples was measured by AccuPycII 1340 (measured for the powder samples, the average values for five experiments were adopted).

Synthesis of Poly(thiourea)s: Poly(thiourea)s were synthesized via either polycondensation of diamine with 1,1-thiocarbonyl diimidazole or polyaddition of diamine with diisothiocyanate, by arranging procedures in the previous reports.[27,33] Here the synthesis of ***m*Ph-PTU** and ***mp*Ph-PTU** has been described.

*Synthesis of Poly(1,3-phenylene thiourea) (**mPh-PTU**)*: To a 5 mL flask was added 1,3-phenylenediamine (324 mg, 3 mmol) and was dissolved in DMF (3 mL). Subsequently, 1,1′-thiocarbonyl diimidazole (594 mg, 3 mmol) was added and was stirred at room temperature for 24 h. After the polymerization, the solution was diluted with DMF (4 mL) and was precipitated in methanol (500 mL). The precipitate was collected through filtration, washed with methanol, and dried in vacuo (at room temperature and 85 °C) to obtain ***m*Ph-PTU** as a whitish powder (0.38 g, 84% yield). SEC (DMF with 10 mM LiCl): $M_w = 1.2 \times 10^4$, $M_w/M_n = 3.0$.

*Synthesis of Poly(1,3-phenylene thiourea-alt-1,4-phenylene thiourea) (**mpPh-PTU**)*: To a 30 mL flask were added 1,4-phenylene diisothiocyanate (640 mg, 3.32 mmol) and 1,3-phenylenediamine (360 mg, 3.32 mmol), were dissolved in DMSO (11.1 mL), and were stirred at room temperature for 24 h. After the polymerization, the solution was diluted with DMF (14 mL) and was precipitated in methanol (800 mL). The precipitate was collected through filtration, washed with methanol, and dried in vacuo (at room temperature and at 70 °C) to obtain ***mp*Ph-PTU** as a whitish powder (0.94 g, 94% yield). SEC (DMF with 10 mM LiCl): $M_w = 1.4 \times 10^5$, $M_w/M_n = 4.8$.

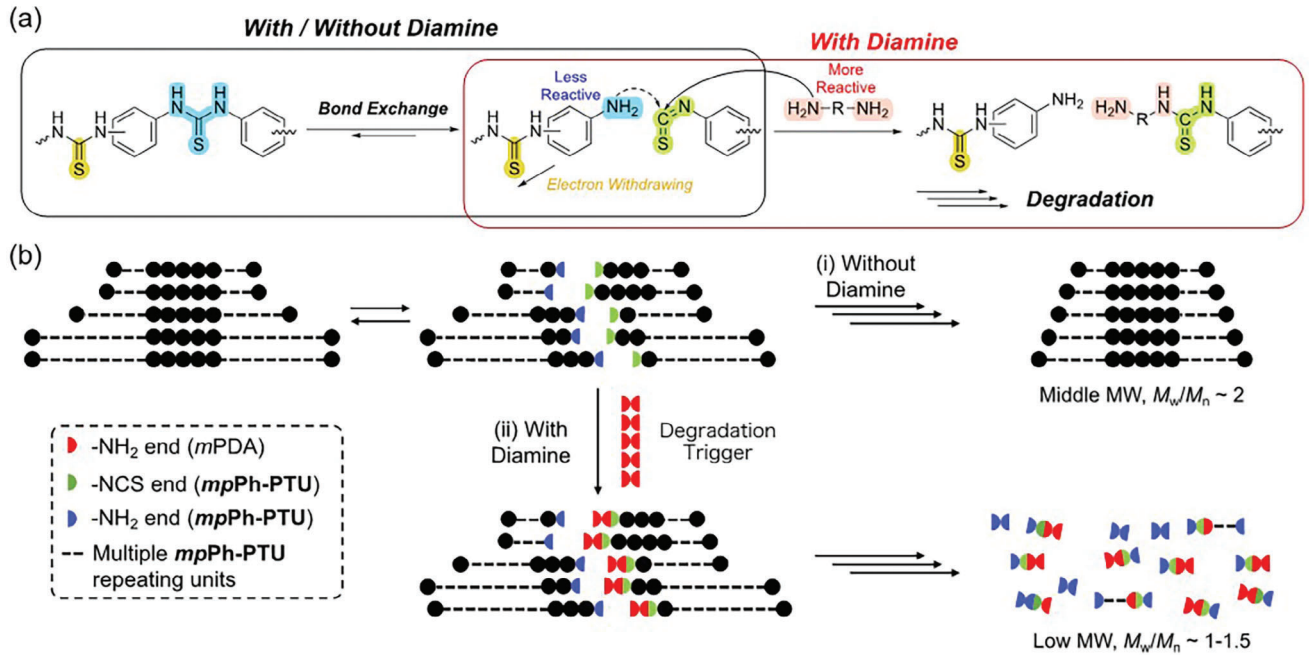

Figure 9. Degradation/redistribution reaction of **PTU**. a) Plausible mechanism for the degradation of ***mp*Ph-PTU** via dynamic covalent chemistry. b) Schematic representation for the length distribution of the polymer chains under the degradation/redistribution reaction with or without diamine (Note: the phenylene spacers were omitted for the clarity).

Variable-Temperature Spectroscopic Ellipsometry: The temperature-dependent *n* and *k* spectra of **PTU**s were obtained by HORIBA UVISEL ER AGMS iHR320 with a Japan Hightec 10 081 hot-stage attachment (incident angle: 75 deg). The samples were measured at room temperature, 50, 70, and 90 °C and were finally cooled to 25 °C at which the ellipsometry was re-measured. During heating/cooling process, the temperature of the hot-stage was changed at the rate of 20 °C min^{-1}, and the samples were measured after standing still for 5 min at the measuring temperature.

Device Fabrication and Measurement: Glass substrates were extensively cleaned using detergent, water, ethanol, and propan-2-ol as solvents in an ultrasonic bath (frequency 37–70 Hz) for 15 min each. Afterward, the slides were dried, and they were positioned in UV–ozone cleaner for 8 min. The clean plates were coated with the desired thickness of PTU via spin coating upon optimization of the deposition protocol. To fabricate the multilayer graphene electrode, three sheets of wafer-scale CVD graphene were synthesized and then stacked on top of each other using a semidry transfer method with polymethyl methacrylate (PMMA) as a support layer. After washout of the latter, 130–140 nm thick layer was obtained via spray coating of PEDOT:PSS solution with a commercial airbrush: N_2 flow at 1 atm, 15 cm distance, and 30 s spraying time. In all the cases, the resulting layers were dried on a hotplate at 120 °C. Active layers were deposited from a sample solution of $[Ir(dtbbpy)(ppy)_2]PF_6$ in acetonitrile (15 mg mL^{-1}) or SY (7 mg mL^{-1} in cyclohexanone) blended with $THABF_4$ (20 mg mL^{-1} in cyclohexanone) in mass ratio SY:$THABF_4$ 1:0.10. The former was spin-coated at 1500 rpm for 30 s while the latter at 2500 rpm for 60 s. In all cases, after the deposition of the active layer, the devices were dried under vacuum for 2 h and transferred to an inert atmosphere glovebox (<0.1 ppm O_2 and H_2O, Angstrom Engineering). Finally, aluminum cathodes were thermally evaporated onto the active layer using a shadow mask under high vacuum (<1×10^{-6} mbar) in an Angstrom Covap evaporator integrated into the inert atmosphere glovebox. Time dependence of luminance, voltage, and current was measured by applying constant or pulsed voltage and monitoring the desired parameters simultaneously using an Avantes spectrophotometer (Avaspec- ULS2048L-USB2) in conjunction with a calibrated integrated sphere Avasphere 30-Irrad and Botest OLT OLED Lifetime-Test System. The device statistics involve up to 20 samples. The thickness of the layers was measured from an AlphaStep 500 profilometer (KLA Tencor) after partial removal of the organic materials with a sharp blade. Topography images were acquired with MFP-3D Origin+ AFM (Asylum Research) and they were elaborated with Gwyddion evaluation software.

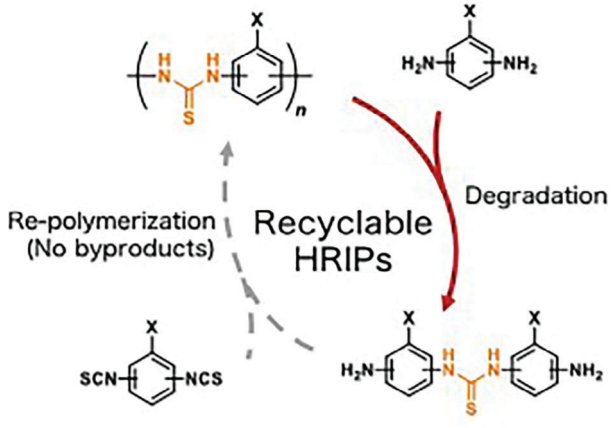

Figure 10. Overview of the future recycling system of **PTU**: Degradation of **PTU** (this study, red) and re-polymerization of the degraded products (future work, grey).

Degradation of PTUs with Diamine: To a 50 mL flask, ***mp*Ph-PTU** (150 mg, 1.0 mmol of thiourea unit) and *m*-phenylenediamine (324 mg, 3.0 mmol) was added, was dissolved in DMF (10 mL), and was stirred at room temperature or at 50 °C. The reaction solution (0.6 mL) was fractionated after 1, 2, 3, 6, 12, 24, 48, 72 h. The fractionated solution was immediately analyzed by SEC chromatograms and ^1H NMR.

PTU Degradation without Diamine Upon Heating: To a 50 mL flask, ***mp*Ph-PTU** (150 mg, 1.0 mmol of thiourea unit) was dissolved in DMF (10 mL) and was stirred at room temperature or at 50 °C (Entry 3 for Figure 7b). The procedures for the fractionation and the ^1H NMR and

SEC measurements were the same as the case of the degradation with diamine.

PTU Degradation without Diamine at Room Temperature: To a 50 mL flask, ***mp*Ph-PTU** (75 mg, 0.5 mmol of thiourea unit) was dissolved in DMF (5 mL) and was stirred at room temperature or at 50 °C (Entry 4 for Figure 7b). The procedures for the fractionation and the ^{1}H NMR and SEC measurements were the same as the case of the degradation with diamine, except that 0.4 mL of the reaction solution was fractionated for each time conditions.

Determination of Degradation Efficiency: In this study, the degradation progress of **PTU** was monitored by determining degradation efficiency, which indicates the ratio of thiourea groups adjacent to the arylamino terminus to all thiourea groups. Here, degradation efficiency can be described as follows:

$$(\text{Degradation efficiency}) = \frac{A_{\text{amino}}}{2A_{\text{thiourea}}} \quad (1)$$

where A_{thiourea} and A_{amino} denote ^{1}H NMR integrals of the signals for all thiourea N—H groups (≈9–10.5 ppm) and terminal NH_2 groups (note that NH_2 groups of the diamines were excluded). (Note: For example, in the case that all adjacent moieties of thiourea groups in the **PTU** chains were fully converted to the arylamino groups, E_{deg} was calculated as 1.00.).

Supporting Information

Supporting Information is available from the Wiley Online Library or from the author.

Acknowledgements

S.W. and L.M.C. contributed equally to this work. This work was partially supported by Grants-in-Aid for Scientific Research (Nos. 21H04695, 22K18335, and 22KJ2927) from MEXT, Japan. S.W. acknowledges the Grant-in-Aid from Waseda Research Institute for Science and Engineering (Early Bird) and Mizuho Foundation for the Promotion of Sciences.The authors thank Dr. Toshimichi Shibue (Waseda univ.) for the VT-NMR measurements and fruitful discussions. This work was the result of using research equipment NMR spectrometer AVANCE 600 NEO (C1029) shared in MEXT Project for promoting public utilization of advanced research infrastructure (Program for supporting construction of core facilities) Grant Number JPMXS0440500023. L.M.C., R.D.C., V.C., and R.R. acknowledged the European Union's innovation programm under grant agreement MSCA-ITN STiBNite No. 956923.

Open access funding enabled and organized by Projekt DEAL.

Conflict of Interest

The authors declare no conflict of interest.

Data Availability Statement

The data that support the findings of this study are available from the corresponding author upon reasonable request.

Keywords

easy degradability, high refractive index, light outcoupling, light-emitting electrochemical cells, polythiourea

Received: March 13, 2024
Published online: April 11, 2024

[1] T. Higashihara, M. Ueda, *Macromolecules* **2015**, *48*, 1915.
[2] J.-G. Liu, M. Ueda, *J. Mater. Chem.* **2009**, *19*, 8907.
[3] H. Ma, A. K.-Y. Jen, L. R. Dalton, *Adv. Mater.* **2002**, *14*, 1339.
[4] T. S. Kleine, R. S. Glass, D. L. Lichtenberger, M. E. Mackay, K. Char, R. A. Norwood, J. Pyun, *ACS Macro Lett.* **2020**, *9*, 245.
[5] E. Kim, H. Cho, K. Kim, T.-W. Koh, J. Chung, J. Lee, Y. Park, S. Yoo, *Adv. Mater.* **2015**, *27*, 1624.
[6] Q. Wei, R. Pötzsch, X. Liu, H. Komber, A. Kiriy, B. Voit, P.-A. Will, S. Lenk, S. Reineke, *Adv. Funct. Mater.* **2016**, *26*, 2545.
[7] J.-H. Kim, N. X. V. Lan, U. Kulkarni, C. Kim, S. M. Cho, P. J. Yoo, D. Kim, M. Schroeder, G.-R. Yi, *Adv. Mater. Interfaces* **2020**, *7*, 2001422.
[8] E. K. Macdonald, M. P. Shaver, *Polym. Int.* **2015**, *64*, 6.
[9] S. Watanabe, K. Oyaizu, *Bull. Chem. Soc. Jpn.* **2023**, *96*, 1108.
[10] Z. Sun, H. Huang, L. Li, L. Liu, Y. Chen, *Macromolecules* **2017**, *50*, 8505.
[11] Y. Hu, L. Zhang, Z. Wang, R. Hu, B. Z. Tang, *Polym. Chem.* **2023**, *14*, 2617.
[12] Y. Zhou, Z. Zhu, K. Zhang, B. Yang, *Macromol. Rapid Commun.* **2023**, *44*, 2300411.
[13] J. J. Griebel, S. Namnabat, E. T. Kim, R. Himmelhuber, D. H. Moronta, W. J. Chung, A. G. Simmonds, K.-J. Kim, J. van der Laan, N. A. Nguyen, E. L. Dereniak, M. E. Mackay, K. Char, R. S. Glass, R. A. Norwood, J. Pyun, *Adv. Mater.* **2014**, *26*, 3014.
[14] M. Lee, Y. Oh, J. Yu, S. G. Jang, H. Yeo, J.-J. Park, N.-H. You, *Nat. Commun.* **2023**, *14*, 2866.
[15] Q. Li, K. L. Ng, X. Pan, J. Zhu, *Polym. Chem.* **2019**, *10*, 4279.
[16] X. Wu, J. He, R. Hu, B. Z. Tang, *J. Am. Chem. Soc.* **2021**, *143*, 15723.
[17] J. M. Scheiger, P. Theato, in *Sulfur-Containing Polymers*, (Eds: X.-H. Zhang, P. Theato), Wiley, Hoboken, New Jersey **2021**, pp. 305–338.
[18] S. Watanabe, K. Oyaizu, *Macromolecules* **2022**, *55*, 2252.
[19] S. Watanabe, T. Takayama, K. Oyaizu, *ACS Polym Au* **2022**, *2*, 458.
[20] S. Watanabe, H. Nishio, T. Takayama, K. Oyaizu, *ACS Appl Polym Mater* **2023**, *5*, 2307.
[21] C. Kim, S. Nakagawa, M. Seshimo, H. Ejima, H. Houjou, N. Yoshie, *Macromolecules* **2020**, *53*, 4121.
[22] S. Mondal, J. J. Lessard, C. L. Meena, G. J. Sanjayan, B. S. Sumerlin, *J. Am. Chem. Soc.* **2022**, *144*, 845.
[23] S. Chen, W. H. Binder, *Acc. Chem. Res.* **2016**, *49*, 1409.
[24] W.-X. Liu, Z. Yang, Z. Qiao, L. Zhang, N. Zhao, S. Luo, J. Xu, *Nat. Commun.* **2019**, *10*, 4753.
[25] R. Custelcean, N. L. Engle, P. V. Bonnesen, *CrystEngComm* **2007**, *9*, 452.
[26] R. Custelcean, *Chem. Commun.* **2008**, 295.
[27] Y. Yanagisawa, Y. Nan, K. Okuro, T. Aida, *Science* **2018**, *359*, 72.
[28] Y. Fujisawa, A. Asano, Y. Itoh, T. Aida, *J. Am. Chem. Soc.* **2021**, *143*, 15279.
[29] S. Dai, J. He, X. Chen, J. Cui, H. Zhao, R. Zhang, H. Lei, J. Yin, L. Cai, F. Ye, X. Kong, R. Hu, M. Huang, *Macromolecules* **2023**, *56*, 3660.
[30] S. Wu, M. Luo, D. J. Darensbourg, X. Zuo, *Macromolecules* **2019**, *52*, 8596.
[31] D. S. Lee, Y.-S. Choi, J. H. Hwang, J.-H. Lee, W. Lee, S.-K. Ahn, S. Park, J.-H. Lee, Y. S. Kim, D.-G. Kim, *ACS Appl Polym Mater* **2021**, *3*, 3714.
[32] S. Wu, W. Li, M. Lin, Q. Burlingame, Q. Chen, A. Payzant, K. Xiao, Q. M. Zhang, *Adv. Mater.* **2013**, *25*, 1734.
[33] Y. Feng, Y. Hasegawa, T. Suga, H. Nishide, L. Yang, G. Chen, S. Li, *Macromolecules* **2019**, *52*, 8781.
[34] Y. Feng, L. Jiang, A. Yang, X. Liu, L. Yang, G. Lu, S. Li, *Macromol. Rapid Commun.* **2022**, *43*, 2100700.
[35] R. Ma, V. Sharma, A. F. Baldwin, M. Tefferi, I. Offenbach, M. Cakmak, R. Weiss, Y. Cao, R. Ramprasad, G. A. Sotzing, *J. Mater. Chem. A* **2015**, *3*, 14845.
[36] S. Watanabe, T. Takayama, H. Nishio, K. Matsushima, Y. Tanaka, S. Saito, Y. Sun, K. Oyaizu, *Polym. Chem.* **2022**, *13*, 1705.

[37] M.-C. Fu, Y. Murakami, M. Ueda, S. Ando, T. Higashihara, *J Polym Sci A Polym Chem* **2018**, *56*, 724.
[38] M.-C. Fu, M. Ueda, S. Ando, T. Higashihara, *ACS Omega* **2020**, *5*, 5134.
[39] S.-Y. Kim, J.-H. Lee, H.-S. Shim, J.-J. Kim, *Org. Electron.* **2013**, *14*, 1496.
[40] T. Chen, X. He, Q. Lu, *ACS Appl Polym Mater* **2023**, *5*, 5436.
[41] Y. Feng, M. Li, K. Shang, H. Niu, G. Qu, G. Lu, S. Li, *Appl. Phys. Lett.* **2023**, *122*, 123902.
[42] G. L. Slonimskii, A. A. Askadskii, A. I. Kitaigorodskii, *Polym. Sci. U.S.S.R.* **1970**, *12*, 556.
[43] a) E. Fresta, R. D. Costa, *J. Mater. Chem. C* **2017**, *5*, 5643; b) E. Fresta, R. D. Costa, *Adv. Funct. Mater.* **2020**, *30*, 1908176.
[44] M. C. Gather, S. Reineke, *J Photonics Energy* **2015**, *5*, 057607.
[45] H. Benisty, R. Stanley, M. Mayer, *J Opt Soc Am A* **1998**, *15*, 1192.
[46] M. Furno, R. Meerheim, S. Hofmann, B. Lüssem, K. Leo, *Phys. Rev. B* **2012**, *85*, 115205.
[47] L. M. Cavinato, K. Yamaoka, S. Lipinski, V. Calvi, D. Wehenkel, R. van Rijn, K. Albrecht, R. D. Costa, *Adv. Funct. Mater.* **2023**, *33*, 2302483.
[48] S. van Reenen, R. A. J. Janssen, M. Kemerink, *Adv. Funct. Mater.* **2012**, *22*, 4547.
[49] J.-Z. Zhao, T.-J. Yue, B.-H. Ren, Y. Liu, W.-M. Ren, X.-B. Lu, *Macromolecules* **2022**, *55*, 8651.
[50] T. Kimura, K. Kuroda, H. Kubota, M. Ouchi, *ACS Macro Lett.* **2021**, *10*, 1535.
[51] Z. Huang, M. Shanmugam, Z. Liu, A. Brookfield, E. L. Bennett, R. Guan, D. E. Vega Herrera, J. A. Lopez-Sanchez, A. G. Slater, E. J. L. McInnes, X. Qi, J. Xiao, *J. Am. Chem. Soc.* **2022**, *144*, 6532.
[52] A. Kazama, Y. Kohsaka, *Polym. Chem.* **2022**, *13*, 6484.
[53] Y. Minami, N. Matsuyama, Y. Takeichi, R. Watanabe, S. Mathew, Y. Nakajima, *Commun Chem* **2023**, *6*, 14.
[54] M. Vlatković, B. L. Feringa, *Tetrahedron* **2019**, *75*, 2188.
[55] H. Feng, N. Zheng, W. Peng, C. Ni, H. Song, Q. Zhao, T. Xie, *Nat. Commun.* **2022**, *13*, 397.
[56] Y. M. Li, Z. P. Zhang, M. Z. Rong, M. Q. Zhang, *Nat. Commun.* **2022**, *13*, 2633.
[57] H. Otsuka, *Polym J* **2013**, *45*, 879.
[58] H. Otsuka, K. Aotani, Y. Higaki, Y. Amamoto, A. Takahara, *Macromolecules* **2007**, *40*, 1429.
[59] T.-J. Yue, L.-Y. Wang, W.-M. Ren, *Polym. Chem.* **2021**, *12*, 6650.